Dual-Energy C-Arm CT in the Angiographic Suite

Sanjit Datta, Jang-Hwan Choi, Christine Niebler, Andreas Maier, Rebecca Fahrig, and Kerstin Müller

***Abstract*—Dual-energy CT techniques have demonstrated tremendous clinical value due to their ability to distinguish materials based on atomic number. C-arm CT is currently used to guide interventional procedures, but there are no commercially available systems that employ dual-energy material decomposition. This paper explores the feasibility of implementing a fast kV-switching technique to perform dual-energy C-arm CT on a clinical angiography system. As an initial proof of concept, a fast kV-switching scan with energies of 90 kV and 125 kV was compared to respective constant kV scans. During rapid kV-switching acquisitions, the energy produced by the tube at each pulse is up to 5% lower than the energy produced during kV-constant acquisitions. The small instability in the produced kV, measured as the standard deviation of the kV produced in each pulse, is up to 4 times higher for kV-switching acquisitions. These minor deficits resulted in a small reduction in contrast resolution of the fast kV-switching 3D reconstructions.**

I. Introduction

A. Purpose of this Work

C-arm angiography systems provide the primary imaging modality used during interventional procedures. These systems are capable of guiding the physician with fluoroscopic 2D X-rays at frame rates up to 30 f/s as well as rotational scans in which X-rays are rapidly acquired through a range of projection angles. Using a cone-beam reconstruction (FDK) algorithm [1], a 3D reconstruction of the field of view can be created from a rotational acquisition. The 3D reconstructions are clinically used for numerous applications, including to identify feeding vessels of a liver tumor in interventional oncology [2] or to assess cerebral aneurysms in neuroradiology [3]. In the last decade, dual-energy imaging in conventional CT has grown in clinical use. This technique allows the differentiation of materials and tissue based on differential absorption of varying X-ray photon energies [4]. For example, the attenuation of iodine, which is used as the intravascular contrast agent for most interventions, decreases more than the attenuation of soft tissue with increasing photon energy. Acquiring X-ray projection images at different photon energies requires a photon-counting energy-discriminating detector (photon counting technique), two simultaneous working X-ray tubes (dual source technique), or one X-ray tube with rapid modulation of the tube voltage (fast-switching technique) [5], [6]. In this paper, we test the hypothesis that fast-switching dual-energy imaging is possible with an interventional C-arm system using only one sweep of the C-arm. The system is equipped with one X-ray tube and one flat-panel detector and can be used to generate images at different energy levels by switching the X-ray tube potential from pulse to pulse. First, kV measurements were performed to prove the concept of kV-switching with the C-arm system as well as to measure any instability resulting from rapidly switching the tube voltage.

S. Datta was with Siemens Healthcare GmbH, Forchheim, Germany at the time of submission and is now with the School of Medicine, Case Western Reserve University, Cleveland, OH. J.-H. Choi, and K. Müller are with the Radiological Sciences Lab, Department of Radiology, Stanford University, Stanford, CA, USA. E-mail: kmuell@stanford.edu. R. Fahrig was with the Radiological Sciences Lab, Department of Radiology, Stanford University, Stanford, CA, USA at the time of submission and is now with Siemens Healthcare GmbH, Forchheim, Germany. C. Niebler is with the Department of Electrical Engineering, Technische Hochschule Nürnberg, Germany. A. Maier is with the Pattern Recognition Lab, Department of Computer Science, Friedrich-Alexander-Universität Erlangen-Nürnberg, Germany.

B. State of the Art

To date, there is no clinical C-arm system available allowing dual-energy imaging with a single rotational sweep. However, dual-energy conventional CT has grown in popularity due to several important capabilities. By differentiating between materials such as iodine, soft tissue, and calcium, dual energy acquisitions can produce volumetric images in which voxels containing those materials are suppressed or enhanced [7]. These calculated images include (a) virtual non-enhanced, with iodine suppressed [8], (b) bone removal [9], with calcium suppressed [10], and (c) virtual subtracted, with only iodine shown [4]. Similarly, modeling the attenuation of each voxel at different energies enables calculation of simulated monoenergetic images which can increase contrast or reduce some types of artifacts.

II. C-arm CT: kV-Switching Setup and Experiments

In general, automatic exposure control (AEC) software is integrated in C-arm systems in order to maintain the same detector entrance dose throughout the scan while rotating around the patient, similar to tube current modulation in conventional CT [11], [12]. The software adapts the current (mA), pulse width (ms), and sometimes energy (kV) in order to maintain a constant detector entrance dose, meaning the exposure varies dynamically based on the projection angle and attenuation of the object in the field of view. This AEC correction algorithm must be disabled in order to manually control the image acquisition parameters. A prototype software application enables manual control of the tube output on an Artis zeego C-arm angiography system (Siemens Healthcare GmbH, Forchheim, Germany). The prototype uses a modifiable configuration file that allows acquisition of projection images with predefined acquisition parameters. Each acquisition resulted in 248 projections over an angular range of 200 degrees with an angular increment of 0.8 °/f. Thus, for the kV-switching scan, there were 124 projections acquired at approximately 90 kV interleaved with 124 projections acquired at approximately 125 kV; these sets of projections were separated and reconstructed

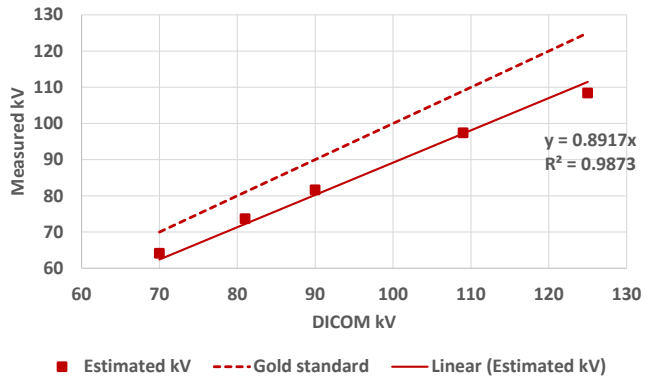

Figure 1: Correlation of kV estimations with the kV meter and the reported kV in the DICOM header for 3D acquisitions with the AEC turned on.

with a filtered-backprojection algorithm at a single energy. To facilitate a head-to-head comparison, constant kV acquisitions were undersampled by removing alternating projections before reconstruction; thus, the number of projections used in each reconstruction remained fixed at 124. The 2D X-ray projection images have a dimension of 1024×960 pixel with an isotropic resolution of 0.3mm. All 2D projection images were pre-processed according to the actual acquisition parameters used. Then, the cone-beam reconstruction was performed offline using a freely-available software framework CONRAD [13]. The image reconstruction was performed on an image volume of $(25.6\text{cm})^3$, distributed on a 256^3 voxel grid.

A. Experiment I

Based on the datasheet of the installed X-ray generator, a variance of $\pm 5\%$ in the generated kV is expected [14]. In order to test the feasibility of the C-arm system reliably delivering the desired kV when rapidly alternating between adjacent frames, the kV was first estimated during normal acquisitions with the AEC switched on. The peak kV was estimated within the beam path using a non-invasive kV meter from *Radcal Corporation (Model 4081 with the 40X5-W Diagnostic sensor)*. The output of the kV meter was recorded using an oscilloscope. Using the kV values listed by the system in the DICOM header as reference, the estimated kV from the meter was compared to the known kV output of the system. The correlation between estimated and DICOM reported kV results are shown in Figure 1. Overall, the kV meter underestimates the kV by approximately 11% over the full range of clinically relevant energies.

B. Experiment II

In the next experiment, the tube output was compared during fast-switching and constant-kV modes using the same setup as in Experiment II-A. The applied mA and ms during the scan can be obtained from the system itself while the kV was estimated with the kV meter. The system hardware limits the rate at which the tube current can change, so the pulse width is the only parameter that can be modulated to maintain the appropriate exposure to the detector.

Table I: Peak voltage generated during kV-constant and kV-switching scans.

Scans	Requested Peak Voltage (kV)	
	90 kV	125 kV
Constant	83.16 $\pm$ 0.14 kV	113.76 $\pm$ 0.84 kV
Switching	82.49 $\pm$ 0.55 kV	108.20 $\pm$ 2.21 kV

Table II: Current generated during kV-constant and kV-switching scans.

Scans	Requested Current (216 mA)	
	90 kV	125 kV
Constant	211.78 $\pm$ 0.91 mA	200.54 $\pm$ 1.93 mA
Switching	211.10 $\pm$ 1.64 mA	209.01 $\pm$ 0.85 mA

Table III: Pulse width generated during kV-constant and kV-switching scans.

Scans	Requested Pulse width (ms)	
	90 kV (12.5 ms)	125 kV (3.2 ms)
Constant	12.51 $\pm$ 0.03 ms	3.21 $\pm$ 0.01 ms
Switching	12.50 $\pm$ 0.06 ms	3.21 $\pm$ 0.00 ms

First, a constant 90 kV (216 mA, 12.5 ms) scan and a constant 125 kV (216 mA, 3.2 ms) scan were acquired. The resulting measurements were compared to a kV-switching scan in which the parameters were alternated frame-to-frame between 90 kV (216 mA, 12.5 ms) and 125 kV (216 mA, 3.2 ms). The results for the kV measurements are shown in Table I. The kV-constant scans have an offset of approx. 8-9% between the requested and estimated kV, which falls within the deviation expected based on Experiment II-A. The difference between the kV-constant and kV-switching scans is less than 1 kV for a 90 kV target and less than 6 kV for a 125 kV target. The standard deviation of the estimated kV, reflecting the instability of the kV from pulse to pulse, was 2-4 times higher for the kV-switching scans than for the kV-constant scans. Table II shows that the deviation in tube current between the constant and kV-switching scans was 0.68 mA (< 1%) for the 90 kV and 8.47 mA (approx. 4%) for the 125 kV. Table III shows the requested and deployed pulse width (ms). The deviation between the constant and kV-switching scans was 0.01 ms (<0.1%) for the 90 kV and not measurable for the 125 kV scan.

C. Experiment III

A 50 ml syringe was filled with 10 mg/ml iodinated contrast (500 mg I) and inserted in the inner disk of the electron density phantom from *CIRS*, with the syringe wrapped in modeling clay to hold it in place. The same three scans as described in Experiment II-B were performed. All four 3D reconstructions were first filtered with a Gaussian filter (radius of 0.5mm) to

Table IV: Contrast-to-noise-ratio in kV-constant and kV-switching scans.

Scans	Requested Peak Voltage (kV)	
	90 kV	125 kV
Constant	2.33 a.u.	1.81 a.u.
Switching	2.20 a.u.	1.61 a.u.

eliminate dominant artifacts from the angular undersampling. Alternatively, a guided noise reduction technique [15] or few-view iterative reconstruction techniques could be applied [16]. In order to measure the contrast-to-noise ratio (CNR), two ROIs in each reconstruction were measured inside the iodine-filled syringe and in the inner disk of the phantom which is equivalent to water (Fig. 2 and Fig. 3). Inside the ROI of the iodine-filled syringe, the mean intensity $\overline{I}_{\text{iod}}$ and the standard deviation σ_{iod} were measured. Within the ROI of the water-equivalent material $\overline{I}_{\text{wat}}$ and σ_{wat} were measured, respectively. The CNR value results in

$$\text{CNR} = \frac{\overline{I}_{\text{iod}} - \overline{I}_{\text{wat}}}{\sqrt{\sigma_{\text{iod}}^2 + \sigma_{\text{wat}}^2}}. \quad (1)$$

Table IV shows the results for the individual scans. The CNR values of the 90 kV scans are slightly higher than the 125 kV scans, which is to be expected due to the k-edge of iodine at low energy. The kV-switching scans result in slightly lower CNR values than the constant-kV scans. Because the 90 kV scans did not use the same dose as the 125 kV scans, however, it is more important to note the differences in CNR at single energies, which show that there is a small contrast penalty resulting from the additional kV instability caused by using the fast-switching technique. The difference images of both reconstructions (Fig. 2c and Fig. 3c) show minimal visible differences between the constant and the kV-switching scans. Future testing will allow for better dose allocation and kV selection in order to optimize the material decomposition capabilities of this technique.

III. Conclusion

In this paper we proved the hypothesis that an angiographic C-arm system is capable of dual-energy acquisitions using the fast kV-switching technique. The major benefit would be to exploit different tissue characterizations by using data collected using only a single C-arm sweep. Future testing will investigate the stability of kV-switching over the full voltage range available on the system and assess the ability of these scans to perform clinically relevant material decomposition.

Disclaimer: The concepts and information presented in this paper are based on research and are not commercially available.

Acknowledgment

The authors gratefully acknowledge funding support from the NIH Shared Instrument Grant S10 RR026714 supporting the zeego@StanfordLab, and Siemens AX.

References

[1] L. A. Feldkamp, L. C. Davis, and J. W. Kress, "Practical cone-beam algorithm," *Journal of the Optical Society of America A*, vol. 1, no. 6, p. 612, 1984.

[2] A. Tognolini, J. Louie, G. Hwang, L. Hofmann, D. Sze, and N. Kothary, "C-arm Computed Tomography for Hepatic Interventions: A Practical Guide," *Journal of Vascular and Interventional Radiology*, vol. 21, pp. 1817–1823, Dec. 2010.

[3] N. S. Heran, J. K. Song, K. Namba, W. Smith, Y. Niimi, and A. Berenstein, "The utility of DynaCT in neuroendovascular procedures," *American Journal of Neuroradiology*, vol. 27, no. 2, pp. 330–332, 2006.

[4] A. Graser, T. R. C. Johnson, H. Chandarana, and M. Macari, "Dual energy CT: Preliminary observations and potential clinical applications in the abdomen," *European Radiology*, vol. 19, no. 1, pp. 13–23, 2009.

[5] C. H. McCollough, S. Leng, L. Yu, and J. G. Fletcher, "Dual- and Multi-Energy CT: Principles, Technical Approaches, and Clinical Applications.," *Radiology*, vol. 276, no. 3, pp. 637–653, 2015.

[6] A. C. Silva, B. G. Morse, A. K. Hara, R. G. Paden, N. Hongo, and W. Pavlicek, "Dual-energy (spectral) CT: applications in abdominal imaging.," *Radiographics : a review publication of the Radiological Society of North America, Inc*, vol. 31, no. 4, pp. 1031–1046; discussion 1047–1050, 2011.

[7] M. Karcaaltincaba and A. Aykut, "Dual-energy CT revisited by multidetector ct: review of principles and clinical applications," *Diagnostic and Interventional Radiology*, no. September 2010, pp. 181–194, 2010.

[8] C. M. Sommer, C. B. Schwarzwaelder, W. Stiller, S. T. Schindera, U. Stampfl, N. Bellemann, M. Holzschuh, J. Schmidt, J. Weitz, L. Grenacher, H. U. Kauczor, and B. a. Radeleff, "Iodine removal in intravenous dual-energy CT-cholangiography: Is virtual non-enhanced imaging effective to replace true non-enhanced imaging?," *European Journal of Radiology*, vol. 81, no. 4, pp. 692–699, 2012.

[9] M. van Straten, M. Schaap, M. L. Dijkshoorn, M. J. Greuter, A. van der Lugt, G. P. Krestin, and W. J. Niessen, "Automated bone removal in CT angiography: Comparison of methods based on single energy and dual energy scans," *Medical Physics*, vol. 38, no. November, p. 6128, 2011.

[10] F. Schwarz, J. W. Nance, B. Ruzsics, G. Bastarrika, A. Sterzik, and U. J. Schoepf, "Quantification of Coronary Artery Calcium on the Basis of Dual-Energy Coronary CT Angiography," *Radiology*, vol. 264, no. 3, pp. 700–707, 2012.

[11] R. Fahrig, R. Dixon, T. Payne, R. L. Morin, A. Ganguly, and N. Strobel, "Dose and image quality for a cone-beam C-arm CT system.," *Medical physics*, vol. 33, no. 12, pp. 4541–4550, 2006.

[12] C. H. McCollough, M. R. Bruesewitz, and J. M. Kofler, "CT dose reduction and dose management tools: overview of available options.," *Radiographics : a review publication of the Radiological Society of North America, Inc*, vol. 26, no. 2, pp. 503–512, 2006.

[13] A. Maier, H. G. Hofmann, M. Berger, P. Fischer, C. Schwemmer, H. Wu, K. Müller, J. Hornegger, J.-H. Choi, C. Riess, A. Keil, and R. Fahrig, "CONRAD–a software framework for cone-beam imaging in radiology.," *Medical physics*, vol. 40, no. 11, p. 111914, 2013.

[14] Siemens Healthcare GmbH, "Artis zeego Owner Manual," tech. rep., 2013.

[15] M. Manhart, R. Fahrig, J. Hornegger, A. Doerfler, and A. Maier, "Guided Noise Reduction for Spectral CT with Energy-Selective Photon Counting Detectors," in *Proceedings of the Third CT Meeting*, pp. 91–94, 2014.

[16] J. Jorgensen, E. Sidky, and X. Pan, "Quantifying Admissible Undersampling for Sparsity-Exploiting Iterative Image Reconstruction in X-Ray CT," *IEEE Transactions on Medical Imaging*, vol. 13, no. 2, pp. 460–473, 2012.

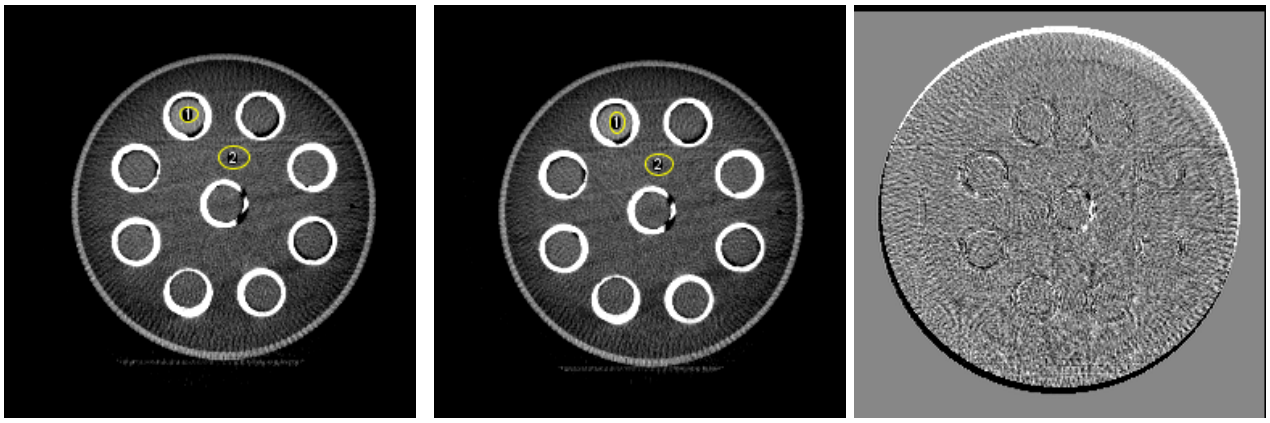

(a) (b) (c)

Figure 2: 3D axial slices of 3D reconstruction of (a) kV-switching scan of 90 kV (b) constant scan of 90 kV (c) difference image (a)-(b). The syringe filled with iodine is measured with ROI1 and the water-based background with ROI2. (a) and (b) HU (C 280 HU, W 1550 HU), (c) window (C 0 HU, W 800 HU).

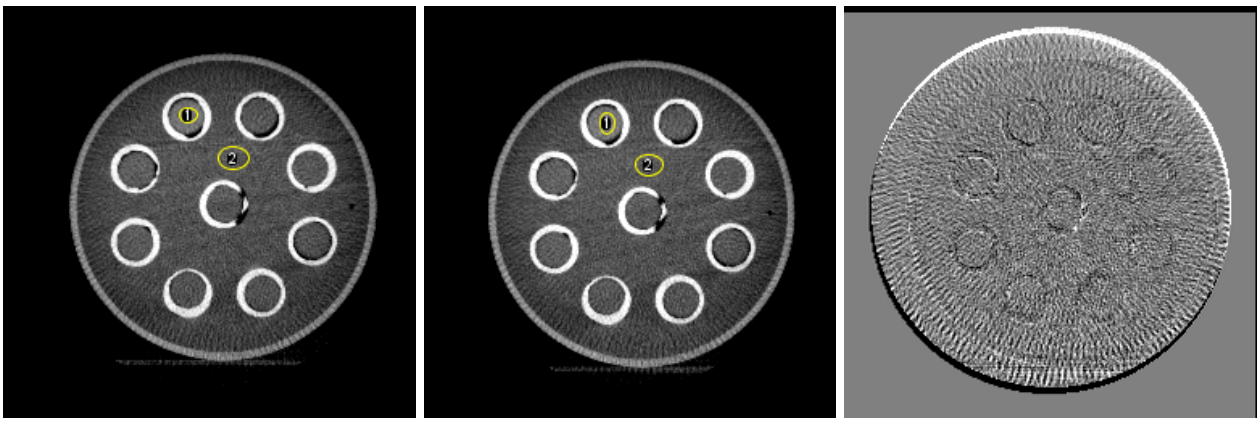

(a) (b) (c)

Figure 3: 3D axial slices of 3D reconstruction of (a) kV-switching scan of 125 kV (b) constant scan of 125 kV (c) difference image (a)-(b). The syringe filled with iodine is measured with ROI1 and the water-based background with ROI2. (a) and (b) HU (C 280 HU, W 1550 HU), (c) window (C 0 HU, W 800 HU).